

Organic Semiconductors

Separation of Electrical and Optical Energy Gaps: Selectively Adjusting the Electrical and Optical Properties for a Highly Efficient Blue Emitter

He Liu, Ping Chen, Dehua Hu, Xiangyang Tang, Yuyu Pan, Huanhuan Zhang, Wenqiang Zhang, Xiao Han, Qing Bai, Ping Lu,* and Yuguang Ma^[a]

Abstract: The design concept of separation of optical and electrical bandgap for wide bandgap materials is further developed in DCzSiPI. The HOMO/LUMO levels can be tuned by incorporation of PI and DCz substituents. The tetraphenylsilane core avoids the intramolecular charge transfer from DCz to PI (DCz = dimer carbazole, PI = phenanthro[9,10-*d*]imidazole). The allowed transitions are found to be from HOMO–1 to LUMO providing DCzSiPI with sufficient bandgap.

Organic semiconductors have already attracted and will continue to attract great interest from researchers worldwide because they have achieved amazing accomplishments in many fields, such as organic lighting-emitting diodes (OLEDs),^[1–7] organic photovoltaics (OPVs),^[8–11] organic field-effect transistors (OFETs),^[12–15] and organic light-emitting electrochemical cells (OLECs).^[16–18] Compared with their inorganic counterparts, the intrinsic low carrier mobilities of organic semiconductors, which result in a limited load-bearing capacity for current, is still an obstacle to further applications. One representative case would be the contradiction between the wide bandgap and effective carrier injection and/or transport properties of semiconductive materials that emit blue or violet light.

Recently, we have demonstrated a novel molecular design strategy to optimize the optical bandgap and carrier injection ability simultaneously in a series of silane-based wide-bandgap materials by independently incorporating electron-donating (carbazole) and electron-accepting (pyridine) moieties.^[19] In this series of wide-bandgap materials, the highest occupied molecular orbital (HOMO) and the lowest unoccupied molecular orbital (LUMO) levels are mainly located on corresponding electron-donating and electron-accepting units, which benefits their carrier injection. However, the allowed electronic transitions are excited from the HOMO to higher energy levels of

the LUMO + *n*, therefore, the whole molecule maintains a wide optical bandgap. The separation of optical and electrical bandgap to achieve wide bandgap and good carrier injection properties simultaneously provides us with a hopeful prospect for the design of organic wide-bandgap materials.

To further develop and investigate the universality of this new design strategy, we herein selectively modified the HOMO and LUMO energy levels of a new series of tetraphenylsilane compounds. We took phenanthro[9,10-*d*]imidazole (PI) as a *n*-type model unit because it has good electron injection property and exhibits blue light emission.^[20–22] The carbazole (Cz) and dimer carbazole (DCz), which are good electron-donating units, were kept unchanged. Through this material design, we developed two new bipolar materials CzSiPI and DCzSiPI to investigate the possibility of adjusting electrical and optical bandgaps independently in these silane-cored compounds. SiPI with only one PI substituent was also synthesized for comparison purposes.

The structures of these three molecules are shown in Figure 1. These materials were synthesized by using a Suzuki coupling and Ullmann reaction (see Scheme S1 in the Support-

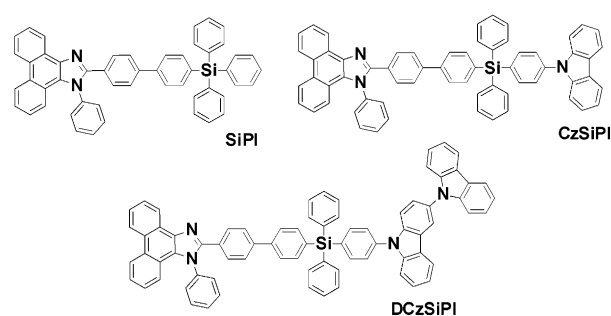


Figure 1. Molecular structures of SiPI, CzSiPI, and DCzSiPI.

ing Information). The chemical structures were fully characterized by using NMR spectroscopy, mass spectrometry, and elemental analysis, and correspond well with their expected structures. All materials showed good thermal stability. There was no obvious glass transition temperature (T_g) of SiPI during the whole heating process, whereas the T_g of CzSiPI and DCzSiPI reached 166 and 198 °C, respectively (Figure S1a in the Supporting Information), which is rarely seen for organic molecules. The decomposition temperatures (T_d) of three com-

[a] Dr. H. Liu, Dr. P. Chen, Dr. D. Hu, X. Tang, Dr. Y. Pan, H. Zhang, W. Zhang, X. Han, Q. Bai, Prof. P. Lu, Prof. Y. Ma
State Key Laboratory of Supramolecular Structure and Materials
Jilin University, 2699 Qianjin Avenue
Changchun, 130012 (P.R. China)
E-mail: lup@jlu.edu.cn

Supporting information for this article is available on the WWW under <http://dx.doi.org/10.1002/chem.201304544>.

pounds were 474, 506, and 550 °C, respectively (Figure S1b in the Supporting Information). The excellent thermal stability of these materials would be beneficial in applications in OLEDs.

CzSiPI and DCzSiPI showed almost the same absorption spectra as SiPI both in solution and film (Figure 2 and Fig-

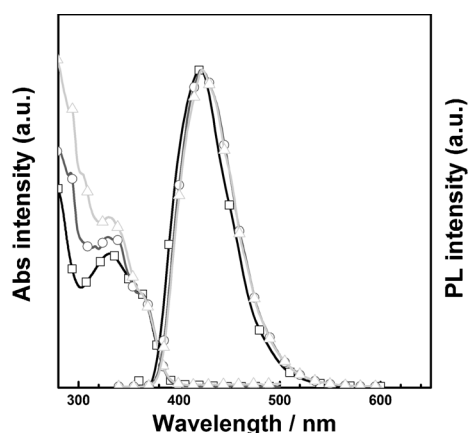


Figure 2. The absorption and PL spectra of SiPI (\square), CzSiPI (\circ), and DCzSiPI (Δ) in dilute CH_2Cl_2 .

ure S2 in the Supporting Information). They all exhibited major absorption bands around $\lambda = 330$ and 365 nm, which arise from the PI unit. The absorption peaks at $\lambda = 292$ and 342 nm are characteristic of the Cz group. Thus, the optical bandgaps (E_{op}) calculated from the absorption edge were 3.19, 3.20, and 3.19 eV for SiPI, CzSiPI, and DCzSiPI, respectively (Table 1). The

	Abs _{max} [nm]		PL _{max} [nm]		PL efficiency [%]		E_{op} [eV] ^[d]	E_{el} [eV] ^[e]
	solution ^[a]	film	solution ^[a]	Film	solution ^[b]	film ^[c]		
SiPI	330, 365	315, 373	422	433	94	77	3.19	3.16
CzSiPI	292, 329, 342, 365	297, 345, 373	422	433	97	65	3.20	3.20
DCzSiPI	293, 331, 343, 365	299, 347, 273	422	433	99	67	3.19	3.09

[a] Recorded in dilute dichloromethane at 10^{-4} M. [b] Compared with quinine sulfate (PL efficiency 54.6% in 0.1 M H_2SO_4). [c] Measured by using an integrated sphere. [d] Calculated from the edge of film absorption spectra. [e] Calculated from the electrochemical data.

photoluminescent (PL) spectra (Figure 2) present the same information. All spectra exhibit blue emission with a maximum peak at $\lambda = 422$ nm in solution and $\lambda = 433$ nm in a film, which suggested that the theoretical transitions and radiations of SiPI, CzSiPI, and DCzSiPI are dominated by the PI chromophore. It is worth noting that there was no low-energy absorption or emission band, which illustrates that additional transitions, such as intramolecular charge-transfer from Cz to PI, did not exist. The p-type Cz unit did not affect the absorption and emission spectra either in CzSiPI or DCzSiPI. This phenomenon is similar to that observed in the donor-acceptor substituted silanes system (CzSiPy and DCzSiPy) that we published previously, in which the n-type pyridine (Py) unit had no effect on the absorption and emission spectra.^[19] This phenomenon that

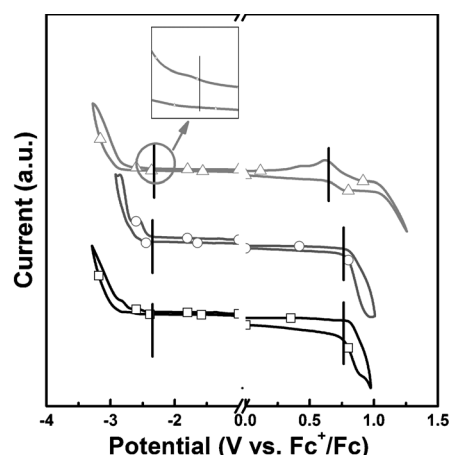


Figure 3. The cyclic voltammetry curves for SiPI (\square), CzSiPI (\circ), and DCzSiPI (Δ) at a scan rate of 100 mV s^{-1} .

E_{op} is dominated by one of the carrier injection units is consistent with our design strategy.

Cyclic voltammetry (CV) was applied to determine the LUMO and HOMO energy levels of these materials (Figure 3). If our design strategy is successful, the reduction process should occur on the electron-deficient PI unit and the oxidation process should be controlled by the electron-rich Cz unit. The obtained experimental results showed that SiPI, CzSiPI, and DCzSiPI indeed underwent the same reduction process, which originated from their n-type PI unit consistent with our molecular design strategy. However, the oxidative onset potential of CzSiPI was the same as SiPI, which suggests that the oxidation

process also occurred on the PI unit rather than on the Cz unit. We found that the HOMO level of PI calculated from the oxidative onset was -5.55 eV, whereas the HOMO level of Cz was -5.61 eV.^[19] Thus PI was more easily oxidized than Cz, which led to the oxidation occurring initially on the PI unit for CzSiPI. For DCzSiPI, the HOMO level of DCz was -5.47 eV,^[19] which is lower than that of PI. Therefore,

the oxidation of DCzSiPI happened on the DCz unit as expected and the HOMO level was calculated to be -5.46 eV. The electrical band gaps (E_{el}) were accordingly found to be 3.16, 3.20, and 3.09 eV for SiPI, CzSiPI, and DCzSiPI, respectively (Table 1). DCzSiPI presented the biggest difference (0.1 eV) between E_{op} and E_{el} ; SiPI and CzSiPI showed differences of 0.03 and 0 eV, respectively. Independently adjusting the energy levels without changing the optical properties was realized in DCzSiPI.

To further understand the spectral and CV behavior, density functional theory (DFT) calculations were carried out at the B3LYP/6-31G level and the distribution of LUMO and HOMO energy levels are shown in Figure 4a. The LUMO levels of all these three materials were located on PI, which corresponds

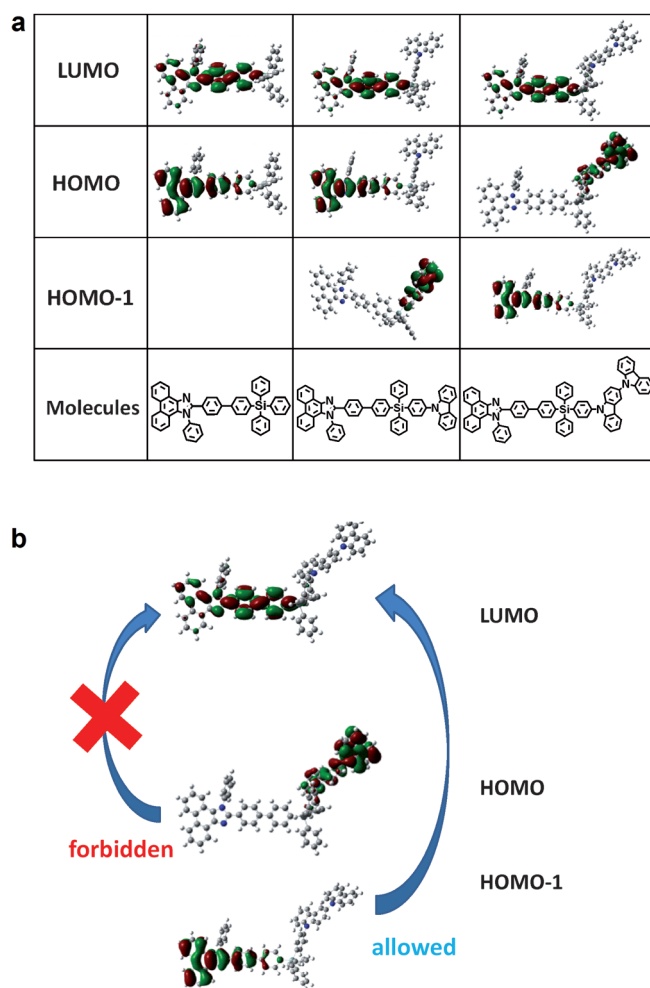


Figure 4. a) The relevant molecular orbital density maps. b) A possible transition sketch map of DCzSiPI.

with the electrochemistry results. The HOMO levels of SiPI and CzSiPI were distributed on PI, whereas the HOMO–1 energy level of CzSiPI is distributed on the Cz unit, which means that Cz has lower oxidative activity than PI. This phenomenon was also consistent with the phenomenon observed by using CV. Unlike the other two molecules, the HOMO of DCzSiPI was spread over the DCz group and exhibited higher oxidative activity than that of PI, whereas the HOMO–1 energy level of DCzSiPI was located on PI and the allowed transitions are from the HOMO–1 to the LUMO (Figure 4b). The result indicated that the separation of optical and electrical bandgap was fully achieved in DCzSiPI.

The special tetrahedral configuration of silane can effectively prevent the donor–acceptor interactions. No charge transfer from donor to acceptor is observed in these bipolar wide-bandgap materials, which is commonly observed in a series of pyridine- and carbazole-substituted silanes we published previously (e.g., CzSiPy).^[19] Their theoretical transitions and radiations are all dominated by one donor or acceptor chromophore, that is, the corresponding carbazole–silane chromophore in CzSiPy and PI–silane in CzSiPI. When full spatial separation

for HOMO and LUMO configuration is obtained, which leads to forbidden transitions between the donor and acceptor (from HOMO to LUMO), for example, in DCzSiPI, then local transitions cause the compound to maintain a high optical bandgap and provide it with sufficient bandgap.

Because all these compounds have the same LUMO level but different hole affinities, the hole-only devices are formed with following structures: ITO/MoO₃ (10 nm)/compounds (60 nm)/MoO₃ (10 nm)/Al (100 nm) (ITO=indium tin oxide) to investigate the hole-injection property. MoO₃ (LUMO = –2.3 eV) was applied to prevent electron injection from Al (–4.3 eV). As shown in Figure S3 in the Supporting Information, the current densities of both CzSiPI and DCzSiPI were much higher than that of SiPI at the same electric field intensity. Introduction of a Cz unit could enhance the hole-transporting ability due to its electron-rich nature. DCzSiPI shows higher current density than CzSiPI because the hole-affinity of DCz was higher than that of Cz. The hole-transporting ability was obviously enhanced by the introduction of a donor unit.

To see how this improvement would affect the electroluminescent properties, light-emitting devices **A–C** were fabricated with the following structures: ITO/PEDOT:PSS/NPB (40 nm)/TCTA (10 nm)/EML (30 nm)/TPBi (40 nm)/LiF (1 nm)/Al (100 nm); PEDOT = poly(3,4-ethylenedioxythiophene), PSS = poly(styrenesulfonate), NPB = *N,N'*-di(1-naphthyl)-*N,N'*-diphenylbenzidine, TCTA = 4,4',4''-tri(*N*-carbazolyl)triphenylamine, EML = emitting layer, TPBi = 1,3,5-tri(1-phenyl-1*H*-benzimidazol-2-yl)benzene. EMLs for devices **A–C** were SiPI, CzSiPI, and DCzSiPI, respectively. NPB and TPBi were used as hole- and electron-transporting layers. TCTA was used as a electron-blocking layer. All the devices exhibited blue emission with maximum peak around $\lambda = 440$ nm (Figure 5). The electroluminescent (EL)

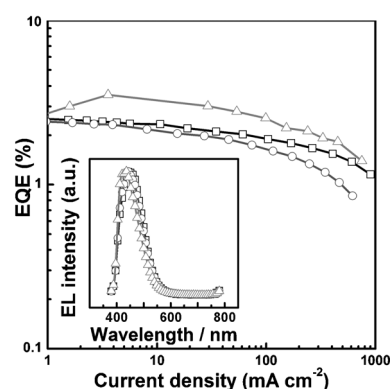


Figure 5. The EQE curves of devices **A** (□), **B** (○), and **C** (△). Inset: the EL spectrum of devices **A** (□), **B** (○), and **C** (△).

spectra for the three compounds were very stable under various driving voltages (Figure S5 in the Supporting Information). As expected, DCzSiPI exhibited the maximum external quantum efficiency (EQE) with a value of 3.5%. To evaluate the influence of charge-balance factor, the use of excitons was calculated according to Equation (1):

$$\eta = \frac{\eta_{\text{ext}}}{\gamma \Phi_p \eta_{\text{out}}} \quad (1)$$

In this equation, η represents the use of excitons for radiative decay, η_{ext} is the external quantum efficiency, γ refers to the ratio of electrons to holes (be regarded as 1), Φ_p is the PL quantum efficiency in solid state, and η_{out} represents the out-coupling efficiency (accounts for 20%). The maximum η calculated for SiPI, CzSiPI and DCzSiPI were 16.2, 19.2, and 26.1%, respectively (Table S2 in the Supporting Information). CzSiPI and DCzSiPI showed lower PL efficiency than SiPI, however, they achieved higher use of excitons than SiPI, which indicates the importance of the charge-balance factor. More balanced carrier injection was achieved and more excitons were used in DCzSiPI and its use of excitons was improved by 61% compared with SiPI. The selectively modified electrical properties of CzSiPI and DCzSiPI have greatly enhanced the EL properties without changing the optical properties.

In conclusion, following the idea to further develop the design concept of separation of the optical and electrical bandgaps for wide-bandgap materials, we synthesized a new series of bipolar materials by using silane to couple electron-donor Cz and electron-acceptor PI units. The HOMO/LUMO levels of the materials can be tuned by the incorporation of PI and Cz substituents. The tetraphenylsilane core prevents the intramolecular charge transfer from donor to acceptor. In DCzSiPI, the allowed transitions are found to be from the HOMO–1 to the LUMO. The separation of the optical and electrical bandgaps is fully achieved in DCzSiPI. DCzSiPI possesses much higher exciton use than SiPI due to the more balanced carrier flux. Our design concept could be very useful for constructing excellent organic semiconductors.

Experimental Section

1-Phenyl-2-(4'-(triphenylsilyl)-(1,1'-biphenyl)-4-yl)-1H-phenanthro[9,10-d]imidazole (SiPI)

In a 100 mL round flask, ethanol (2.5 mL) and K_2CO_3 (2 M, 2.5 mL) were added to a solution of (4-bromophenyl)triphenylsilane (713 mg, 1.65 mmol) and 1-phenyl-2-(4-(4,4,5,5-tetramethyl-1,3,2-dioxaborolan-2-yl)phenyl)-1H-phenanthro[9,10-d]imidazole (821 mg, 1.65 mmol) in toluene (5 mL). $[\text{Pd}(\text{PPh}_3)_4]$ (38 mg, 0.033 mmol) was added and the resultant solution was degassed and stirred at 90 °C for 2 d under nitrogen. Water was added to quench the reaction, the mixture was then extracted with dichloromethane and the organic solution was washed with water and dried over anhydrous sodium sulfate. The crude product was purified by using column chromatography with ethyl petroleum ether/dichloromethane (v/v 1:1) as the eluent to give a white solid (0.72 g, yield: 62%). ^1H NMR (500 MHz, $[\text{D}_6]$ DMSO, 25 °C, TMS): δ = 8.96–8.94 (d, J = 8.4 Hz, 1H, Ar-H), 8.91–8.89 (d, J = 8.2 Hz, 1H, Ar-H), 8.73–8.72 (d, J = 7.6 Hz, 1H, Ar-H), 7.81–7.70 (m, 13H, Ar-H), 7.59–7.46 (m, 18H, Ar-H), 7.37–7.34 (t, J = 8.0 Hz, J = 7.6 Hz, 1H, Ar-H), 7.10–7.08 ppm (d, J = 8.2 Hz, 1H, Ar-H); ^{13}C NMR (125 MHz, CDCl_3 , 25 °C, TMS): δ = 141.2, 136.9, 136.4, 134.1, 133.6, 130.3, 129.9, 129.8, 129.7, 129.3, 129.2, 128.3, 128.2, 127.9, 127.3, 126.4, 126.3, 125.7, 125.0, 124.2, 123.1, 122.9, 120.9 ppm; elemental analysis calcd (%) for $\text{C}_{51}\text{H}_{36}\text{N}_2\text{Si}$: C 86.89, H

5.15, N 3.97; found: C 85.56, H 4.97, N 3.92; MS (55 eV): m/z calcd for $\text{C}_{51}\text{H}_{36}\text{N}_2\text{Si}$: 704.93; found: 705.50 (100) $[\text{M}+\text{H}]^+$.

2-(4'-((4-(9H-Carbazol-9-yl)phenyl)diphenylsilyl)-(1,1'-biphenyl)-4-yl)-1-phenyl-1H-phenanthro[9,10-d]imidazole (CzSiPI)

9-(4-((4-Bromophenyl)diphenylsilyl)phenyl)-9H-carbazole was reacted with 1-phenyl-2-(4-(4,4,5,5-tetramethyl-1,3,2-dioxaborolan-2-yl)phenyl)-1H-phenanthro[9,10-d]imidazole in a Suzuki coupling reaction. The process was the same as SiPI. The crude product was purified by using column chromatography with petroleum ether/dichloromethane (v/v 1:1) as the eluent to give a white solid (0.43 g, yield: 33%). ^1H NMR (500 MHz, CDCl_3 , 25 °C, TMS): δ = 8.95–8.94 (s, 1H, Ar-H), 8.82–8.80 (d, J = 8.7 Hz, 1H, Ar-H), 8.32–8.31 (s, 1H, Ar-H), 8.22–8.21 (d, J = 7.9 Hz, 2H, Ar-H), 8.16–8.13 (d, J = 7.9 Hz, 1H, Ar-H), 7.92–7.90 (d, J = 8.2 Hz, 2H, Ar-H), 7.81–7.42 (m, 37H, Ar-H), 7.37–7.31 (m, 4H, Ar-H), 7.22–7.20 ppm (d, J = 7.6 Hz, 1H, Ar-H); ^{13}C NMR (125 MHz, CDCl_3 , 25 °C, TMS): δ = 141.5, 140.6, 139.1, 137.9, 137.0, 136.4, 133.8, 133.5, 133.2, 130.3, 129.9, 129.8, 129.2, 128.33, 128.26, 128.1, 127.4, 126.9, 126.6, 126.3, 126.2, 126.0, 125.0, 124.2, 123.5, 123.1, 120.9, 120.3, 120.1 ppm; elemental analysis calcd (%) for $\text{C}_{63}\text{H}_{43}\text{N}_3\text{Si}$: C 89.96, H 4.98, N 4.83; found: C 90.11, H 4.88, N 5.07; MS (89 eV): m/z calcd for $\text{C}_{63}\text{H}_{43}\text{N}_3\text{Si}$: 870.12; found: 871.10 (100) $[\text{M}+\text{H}]^+$.

2-(4'-((4-(9H-[3,9'-Bicarbazol]-9-yl)phenyl)diphenylsilyl)-(1,1'-biphenyl)-4-yl)-1-phenyl-1H-phenanthro[9,10-d]imidazole (DCzSiPI)

9-(4-((4-Bromophenyl)diphenylsilyl)phenyl)-9H-3,9'-bicarbazole was reacted with 1-phenyl-2-(4-(4,4,5,5-tetramethyl-1,3,2-dioxaborolan-2-yl)phenyl)-1H-phenanthro[9,10-d]imidazole in a Suzuki coupling reaction. The process was the same as SiPI. The crude product was purified by using column chromatography with petroleum ether/dichloromethane (v/v 1:1) as the eluent to give a white solid (0.43 g, yield: 58%). ^1H NMR (500 MHz, CDCl_3 , 25 °C, TMS): δ = 8.83–8.81 (d, J = 8.2 Hz, 1H, Ar-H), 8.76–8.74 (d, J = 8.4 Hz, 1H, Ar-H), 8.76–8.74 (d, J = 8.5 Hz, 1H, Ar-H), 7.84–7.83 (d, J = 8.2 Hz, 2H, Ar-H), 7.87–7.86 (d, J = 8.2 Hz, 2H, Ar-H), 7.81–7.59 (m, 21H, Ar-H), 7.56–7.44 (m, 11H, Ar-H), 7.34–7.30 (m, 3H, Ar-H), 7.24–7.22 ppm (d, J = 8.2 Hz, 1H, Ar-H); elemental analysis calcd (%) for $\text{C}_{75}\text{H}_{50}\text{N}_4\text{Si}$: C 87.01, H 4.87, N 5.41; found: C 86.29, H 5.09, N 5.26; MS (89 eV): m/z calcd for $\text{C}_{75}\text{H}_{50}\text{N}_4\text{Si}$: 1034.38; found: 1036.50 (100) $[\text{M}+\text{H}]^+$.

Acknowledgements

This work was financially supported by the National Basic Research Program of China (973 Program, 2013CB834701, 2013CB834800), the National Science Foundation of China (grant nos. 21174050, 21374038), and the Graduate Innovation Fund of Jilin University (grant no. 20121044).

Keywords: bipolar • carbazole • donor–acceptor systems • silanes • bandgap

- [1] C. W. Tang, S. A. VanSlyke, *Appl. Phys. Lett.* **1987**, *51*, 913–915.
- [2] Y. J. Pu, G. Nakata, F. Satoh, H. Sasabe, D. Yokoyama, J. Kido, *Adv. Mater.* **2012**, *24*, 1765–1770.
- [3] W. J. Li, D. D. Liu, F. Z. Shen, D. G. Ma, Z. M. Wang, T. Feng, Y. X. Xu, B. Yang, Y. G. Ma, *Adv. Funct. Mater.* **2012**, *22*, 2797–2803.
- [4] H. Liu, G. Cheng, D. H. Hu, F. Z. Shen, Y. Lv, G. N. Sun, B. Yang, P. Lu, Y. G. Ma, *Adv. Funct. Mater.* **2012**, *22*, 2830–2836.

- [5] H. Uoyama, K. Goushi, K. Shizu, H. Nomura, C. Adachi, *Nature* **2012**, *492*, 234–240.
- [6] H. Sasabe, J. Kido, *J. Mater. Chem. C* **2013**, *1*, 1699–1707.
- [7] G. Cheng, Y. Chen, C. L. Yang, W. Lu, C. M. Che, *Chem. Asian J.* **2013**, *8*, 1754–1759.
- [8] G. Yu, J. Gao, C. Hummelen, F. Wudl, A. J. Heeger, *Science* **1995**, *270*, 1789–1791.
- [9] C. J. Brabec, S. Gowrisanker, J. J. M. Halls, D. Laird, S. J. Jia, S. P. Williams, *Adv. Mater.* **2010**, *22*, 3839–3856.
- [10] Z. He, C. Zhang, X. F. Xu, L. J. Zhang, L. Huang, J. W. Chen, H. B. Wu, Y. Cao, *Adv. Mater.* **2011**, *23*, 3086–3089.
- [11] Z. C. He, C. M. Zhong, X. Huang, W. Y. Wong, H. B. Wu, L. W. Chen, S. J. Su, Y. Cao, *Adv. Mater.* **2011**, *23*, 4636–4643.
- [12] J. Zaumseil, H. Sirringhaus, *Chem. Rev.* **2007**, *107*, 1296–1323.
- [13] J. H. Seo, E. B. Namdas, A. Gutacker, A. J. Heeger, G. C. Bazan, *Adv. Funct. Mater.* **2011**, *21*, 3667–3672.
- [14] X. Y. Wang, H. R. Lin, T. Lei, D. C. Yang, F. D. Zhuang, J. Y. Wang, S. C. Yuan, J. Pei, *Angew. Chem.* **2013**, *125*, 3199–3202; *Angew. Chem. Int. Ed.* **2013**, *52*, 3117–3120.
- [15] L. Q. Li, P. Gao, M. Baumgarten, K. Müllen, N. Lu, H. Fuchs, L. F. Chi, *Adv. Mater.* **2013**, *25*, 3419–3425.
- [16] Q. B. Pei, G. Yu, C. Zhang, Y. Yang, A. J. Heeger, *Science* **1995**, *269*, 1086–1088.
- [17] C. V. Hoven, H. P. Wang, M. Elbing, L. Garner, D. Winkelhaus, G. C. Bazan, *Nat. Mater.* **2010**, *9*, 249–252.
- [18] S. Tang, J. Y. Pan, H. A. Buchholz, L. Edman, *J. Am. Chem. Soc.* **2013**, *135*, 3647–3652.
- [19] D. H. Hu, F. Z. Shen, H. Liu, P. Lu, Y. Lv, D. D. Liu, Y. G. Ma, *Chem. Commun.* **2012**, *48*, 3015–3017.
- [20] Z. M. Wang, P. Lu, S. M. Chen, Z. Gao, F. Z. Shen, W. S. Zhang, Y. X. Xu, H. S. Kwok, Y. G. Ma, *J. Mater. Chem.* **2011**, *21*, 5451–5456.
- [21] H. H. Chou, Y. H. Chen, H. P. Hsu, W. H. Chang, Y. H. Chen, C. H. Cheng, *Adv. Mater.* **2012**, *24*, 5867–5871.
- [22] Z. Gao, Y. L. Liu, Z. M. Wang, F. Z. Shen, H. Liu, G. N. Sun, L. Yao, Y. Lv, P. Lu, Y. G. Ma, *Chem. Eur. J.* **2013**, *19*, 2602–2605.

Received: November 20, 2013

Revised: December 11, 2013

Published online on January 29, 2014